What is climate change doing in Himalaya? Thirty years of the Pyramid Meteorological Network (Nepal)

Franco Salerno[1,2,*,°‡], Nicolas Guyennon[3,**,°‡], Nicola Colombo[4], Maria Teresa Melis[5,6], Francesco Gabriele Dessì[5], Gianpietro Verza[5], Kaji Bista[7], Ahmad Sheharyar[1], Gianni Tartari[2]

1 National Research Council, Institute of Polar Sciences, ISP-CNR, Milan, Italy
2 National Research Council, Water Research Institute, IRSA-CNR, Brugherio (MB), Italy
3 National Research Council, Water Research Institute, IRSA-CNR, Montelibretti (Roma), Italy
4 Department of Agricultural, Forest and Food Sciences, University of Turin, Grugliasco, Italy
5 Ev-K2-CNR, Bergamo, Italy
6 Departmento of Chemical and Geological Sciences, Univerity of Cagliari, Monserrato (CA), Italy
7 Nepal Academy of Science and Technology (NAST), Kathmandu, Nepal

* Correspondence: Franco Salerno (franco.salerno@cnr.it); Nicolas Guyennon**(nicolas.guyennon@irsa.cnr.it)
°‡ Franco Salerno and Nicolas Guyennon equally contributed to this paper.

Abstract

Climate change is deeply impacting mountain areas around the globe, especially in Himalaya. However, the lack of long-term meteorological observations at high elevations poses significant challenges to understand and predict impacts at various scales. This also represents a serious limit for model-based projections of future behavior of crucial elements of the mountain cryosphere such as glaciers. Here, we present the Pyramid Meteorological Network, located in Himalaya (Nepal), on the southern slopes of Mt. Everest. The network is composed of 7 meteorological stations located between 2660 and 7986 m a.s.l., which have collected continuous climatic data during the last 30 years (1994-2023). In this paper, we provide details regarding instrument types and characteristics as well as data quality control and assessment. The obtained data series are available on a newly created geoportal. We leverage these unique records to present new knowledge on the Himalayan climate, benefiting also from the highest observational climatic series in the world (Pyramid station, located at above 5000 m a.s.l., close to the Khumbu Glacier). These data will provide fundamental knowledge on climate dynamics in Himalaya that will inform research at high elevations in the coming years. The dataset

is freely accessible from https://geoportal.mountaingenius.org/portal/ (https://zenodo.org/records/15211352; Salerno et al., 2024).

1 **Introduction**

Global temperature has been increasing at unprecedented rates during the last decades, impacting both natural and human systems. Alpine biomes, among the most sensitive natural ecosystems to climate warming, have shown rapid shifts of species distribution ranges and modulations of species interactions (e.g., Sigdel et al., 2021). Furthermore, Himalayan glaciers have been losing mass in the last decades (Biemans et al., 2019; The GlaMBIE Team, 2025). The current uncertainties concerning the glacial shrinkage in the Himalayas are mainly attributed to the lack of measurements of climatic forcings (e.g., Bhattacharya et al., 2021). Indeed, recent research has underlined the need for fine scale investigations, especially at high elevation, to better model the glacio-hydrological dynamics (Yao et al., 2022). In addition, according to Yang et al. (2018), reliable meteorological data at glacial elevations are essential to: (1) place the observed glacial changes in the context of current climatic change, (2) understand hydro-meteorological relationships in cryospheric environments, and (3) calibrate dynamically and statistically downscaled climate fields. However, there are only a few high-elevation weather stations where the glaciers are located, especially in Himalaya. This can be attributed to the remote location of glaciers and the rugged terrain, which make physical access difficult (e.g., Salerno et al., 2015; Lin et al., 2021; Wagnon et al., 2021; Matthews et al., 2022).

As a consequence of the remoteness and difficulty in accessing several high-elevation sites combined with the complications of operating automated weather stations (AWSs) in remote areas, long-term measurements are challenging (Yang et al., 2018). For instance, in Himalaya, meteorological stations at high elevations are extremely scarce (Pepin et al., 2015; Salerno et al., 2015; Matthews et al., 2022). Therefore, in several studies, climatic data at high elevations had to be estimated using low-elevation data (Shrestha et al., 2014; Zhang et al., 2015), which are more common. This is the case of the Central Himalaya, where the Department of Hydrology and Meteorology of Nepal (www.dhm.gov.np/) maintains more than 300 long-term rain stations, although they are mainly located below 3000 m a.s.l.

In this context, in the early 1990s, the Pyramid Meteorological Network was created by the Italian *Ev-K2-CNR Committee* (www.evk2cnr.org). This network is composed of 7 automatic weather stations located on the southern side of Mt Everest (along the Khumbu Valley), in the Central Himalaya (Sagarmatha National Park - SNP; Amatya et al., 2010; Salerno et al., 2010) ranging from 2660 to 7986 m a.s.l.. For each station, the following variables are collected on an hourly basis: air temperature, total precipitation, relative humidity, atmospheric pressure, and wind speed and direction.

Here, we present the overall data set of the Pyramid Meteorological Network and the database in which all meteorological data are stored, freely accessible from https://geoportal.mountaingenius.org/portal/ ~~(https://zenodo.org/records/15211352), and~~(https://zenodo.org/records/15211352). Furthermore, we explore the small-scale climate variability of the longest time series of the network, the Pyramid station (5035 m a.s.l.), located close to the Khumbu Glacier.

2 Region of investigation

Salerno et al. (2015) described the ground network of automatic weather stations (AWSs) belonging to the Pyramid Meteorological Network, which is located on the southern side of Mt Everest (along the Khumbu Valley), in Central Himalaya (Sagarmatha National Park - SNP; Amatya et al., 2010; Salerno et al., 2010) (Fig. 1). The land-cover classification shows that almost one-third of the territory is characterised by glaciers and ice cover, while less than 10% of the park area is forested (*Abies spectabilis*, *Betula utilis*) (Magnani et al., 2018; Pandey et al., 2020). The tree line is located at approx. 4050 m a.s.l., while the landscape is dominated by alpine tundra and lichen above this elevation (Bhuju et al., 2010; Sigdel et al., 2021). Glacial surfaces are distributed from 4300 to above 8000 m a.s.l. Around 75% of the glacier surfaces are located between 5000 and 6500 m a.s.l. (Thakuri et al., 2014, 2016), and ca. 25% of the glacierised area is debris-covered (Shea et al., 2015; Salerno et al., 2017). Glaciers in this area are classified as the summer-accumulation type, which are fed mainly by summer monsoon precipitation (Tartari et al., 2008; Ueno et al., 2008).

The climate in the South Asia and Himalayan region has a strong annual cycle, with the South Asian monsoon that is a phase of this annual cycle. During the pre-monsoon season (March-April-May), the westerlies prevail over this region and are deflected when

crossing the Himalayan mountains. During the monsoon season (June-July-August-September), the westerlies move northward, while south-westerly flows dominate the upper level of the atmosphere and south-easterly flows from Bay of Bengal dominate the lower level (Ichiyanagi et al., 2007). After the offset of the monsoon, the south-westerly and south-easterly flows are replaced by the westerlies. The warm area moves to the south and both air temperature and humidity decrease considerably. Cooling and drying are further enhanced towards the winter (Yang et al., 2018).

Regarding the precipitation, the measurements at Pyramid station (5035 m a.s.l. - Z5035) show that 90% is concentrated from June to September, while the probability of snowfall during these months is very low (4%); the annual cumulative precipitation at this elevation is 446 mm, with a mean annual temperature of –2.5 °C (Salerno et al., 2015). Precipitation linearly increases up to an elevation of 2500 m a.s.l. and exponentially decreases at higher elevations (Salerno et al., 2015). Finally, the wind regime of the area is characterised by up-valley winds during the day throughout the year, while weak up-valley winds occur at night during the monsoon season, with some evidence of down-valley winds occurring at night in the winter (Potter et al., 2018 and references therein reported). Strong diurnal katabatic winds also occur at higher elevations (above ca. 4500 m a.s.l.) due to enhanced glacier melting under warm atmospheric conditions (Salerno et al., 2023).

3 Data and methods

3.1 Weather stations

The first automatic weather station (AWS0) was installed in October 1993, near the Pyramid Laboratory, at 5035 m a.s.l. (Fig. 1, 2; Bertolani et al., 2000). AWS0 recorded temperature data until December 2005. A new station (AWS1) was installed just a few tens of meters away from AWS0 and it has been operating since October 2000. The comparison between the two stations during the overlapping period is detailed in Fig. S1 and Fig. S2. The other stations were installed in the following years in the Khumbu Valley (Fig. 1, Tab. 1). In 2008, the network included seven monitoring sites, including the highest weather station of the world, located at South Col of Mt. Everest (7986 m a.s.l.). The locations of all stations are presented in Figure 1, while Figure 3 shows the temporal availability of the meteorological data. AWS3 (2660 m a.s.l. - Z2660) and AWS5 (5370

m a.s.l. - Z3570) are located below the tree line, while AWS2 (Z4260) is located close to the upper limit of the vegetation. At higher elevation, AWS0 and AWS1 (Z5035) are close to the glacier front elevation, AWS4 (Z5600) is situated at the mean elevation of glaciers and, finally, AWSCC (Z7986) characterizes the highest peaks.

Recently, a new meteorological network was established in the Khumbu Valley by the 2019 National Geographic and Rolex Everest Expedition (https://datadash.appstate.edu/high-altitude-climate/#download), with 5 stations ranging from 3810 to 8810 m a.s.l. (Matthews et al., 2022). On average, this network is located at an elevation higher than the Pyramid Meteorological Network, representing mainly the accumulation zone of the glaciers in the region. Moreover, the GLACIOCLIM group manages some stations on Changri Nup and Mera Glacier (e.g., Wagnon et al., 2021).

3.2 Data description

The list of measured variables, as well as sensors' types and accuracy for each station is presented in Table 3. The ~~database~~dataset contains: AT: 2m Atmospheric Temperature (°C), RR: Rainfall Rate (mm), RH: Relative Humidity (%), AP: Atmospheric Pressure (hPa), WS: Wind Speed (m/s), WD: Wind Direction (°). All times are local time (Nepal Standard Time (NPT), UTC + 5:45). All data are published on an hourly basis. These hourly data are published without any gap filling procedure, when the data is missing the field is empty.

The existence of a permanent laboratory at 5035 m a.s.l. (the Pyramid Laboratory) has allowed constant maintenance for over three decades thanks to the presence of a technician all year round, which resulted in all stations being currently fully operational. In addition, starting from 2024, all stations have been transmitting data which will further limit the issues of missing data in the future. However, the main weakness of this data network is the lack of heated rain gauges, although precipitation is concentrated in summer when minimum temperatures are above +0 °C. According to Salerno et al. (2015), the underestimation of precipitation falling as snow during the remaining months should not be over 20%.

Here we also report the reconstructed monthly Pyramid time series (1994-2023 period) for Tmin (minimum air temperature), Tmax (maximum air temperature), Tmean (mean air temperature), and Prec (precipitation), after the gap filling procedure reported

in §section 3.4. These time series are presented and discussed in §section 4 and §section 5.

3.3 Geoportal structure

Since the early 1990s, when the Pyramid Meteorological Network was created, the Ev-K2-CNR Committee has promoted the sharing of data collected from high-elevation AWSs. In 2014, the first data sharing system was born, and it was called SHARE (Station at High Altitude for Research on the Environment) Geonetwork. The system collected data from 15 stations spread across four countries (Nepal, Pakistan, Italy, and Uganda). The system was designed for open data management, in line with international directives and standards for free access to environmental data. Furthermore, based on a customisation of the GeoNetwork software system, a hierarchical database of the individual stations and sensors was created (Melis et al., 2013; Locci et al., 2014).

In the last ten years, this web platform has been improved according to new digital standards and software release. Furthermore, the publication of station data was accompanied by a new web-GIS platform to provide three services: 1) a structured metadata and data archive, 2) a simplified interface to provide access to AWSs' data, and 3) a dedicated webGIS platform for geo-referenced data. The new GeoPortal is accessible at the address https://geoportal.mountaingenius.org/portal/.

An exclusive function provided by the GeoPortal is the direct access to dataset and databases through a dedicated search data-tab in the portal main menu. Dataset acquired by the projects are stored in a PostgreSQL DBMS: registered GeoPortal users can query the data by the Search Data command, and in the results page, it is possible to proceed to direct download dataset in csv format or to directly consult them in forms of tables and charts. All information provided by the portal is supplied with their relative metadata. The metadata database is the core of the system: only through metadata it is possible to search and retrieve resources. The main search window allows to search any string occurrence in the metadata database: through the result page it is possible to access directly to the metadata sheet with description of resource. Here it is possible to retrieve the direct connection with datasets with the possibility of a direct download of the supplied dataset, accordingly with the file format. Metadata and datasets are strictly related with a two-ways connection.

3.4 Data gap filling for temperature and precipitation time series

The Pyramid station has data gaps corresponding to ca. 10% and 15% for temperature and precipitation, respectively (Table 2). In this study, we applied the same gap filling method (quantile mapping) used for missing data in Salerno et al. (2015), but extending the time series to 2023. All the stations belonging to the network were tested and used for filling the gaps according to a priority criterion based on the degree of correlation among data. AWS1 was chosen as the reference station given the length of the time series and the fact that it is currently still operating. The selected filling method is a simple regression analysis based on quantile mapping (e.g., Déqué, 2007; Themeßl et al., 2012). This regression method has been preferred to more complex techniques, such as the fuzzy rule-based approach (Abebe et al., 2000) or the artificial neural networks (Coulibaly and Evora, 2007; Abudu et al., 2010), considering the peculiarity of this case study where all stations are located in the same valley (Khumbu Valley). This aspect confines the variance among the stations to the elevational gradient of the considered variable, which can be easily reproduced by the stochastic link created by the quantile mapping method. In case all stations registered a simultaneous gap, we applied a multiple imputation technique (Schneider, 2001) that uses other proxy variables to fill the remaining missing data. The uncertainty introduced by the filling process on the Sen's slope (SS) was estimated through a Monte Carlo uncertainty analysis. Details on the reconstruction procedure and the computation of the associated uncertainty are provided in Salerno et al. (2015).

3.5 Statistical analyses

In this study, we applied the Mann–Kendall test (MK, Kendall, 1975) at the monthly scale (after daily data aggregation) to analyse the non-stationarity of meteorological data. This test is widely adopted to assess significant trends in hydrometeorological time series (Guyennon et al., 2013). The MK test is non-parametric, thus being less sensitive to extreme sample values and it is independent from the hypothesis about the nature of the trend, whether linear or not. The MK test verifies the assumption of the stationarity of the investigated series by ensuring that the associated normalized

Kendall's tau-b coefficient, $\mu(\tau)$, is included within the confidence interval for a given significance level (for $\alpha = 5\%$, the $\mu(\tau)$ is below −1.96 and above 1.96). We used the Sen's slope (SS) proposed by Sen (1968) as a robust linear regression allowing the quantification of the potential trends revealed by the MK. The significance level is established for $p < 0.05$. We defined a slight significance for $p < 0.10$. The uncertainty associated with the SS (1994–2013) is estimated through a Monte Carlo uncertainty analysis (James and Oldenburg, 1997). In the sequential form (seqMK) $\mu(\tau)$ the test is applied forward starting from the oldest values (progressive trend) and backward starting from the most recent values (retrograde trend). The crossing period allows us to identify the approximate starting point of the trend. In this study, we applied the seqMK to monthly vectors. To monitor the seasonal non-stationarity, we reported the monthly progressive $\mu(\tau)$ with a pseudo color code, where the warm colors represent the positive slopes and cold colors the negative ones

4 Results of the reconstructed time series

At 5035 m a.s.l., the precipitation is concentrated in the period June–September (87.7%, Fig. 4) and, considering that the minimum daily temperature during these months is above +0 °C, the probability of snowfall is very low. According to Salerno et al. (2015), the underestimation of precipitation falling as snow during the remaining months ~~should not be over~~ is likely below 20%. Sustained by this analysis results, we performed the precipitation trend analysis focusing on the warmest months (Fig. 5d).

Trend analysis at high elevation

Figure 5 shows the reconstructed Pyramid time series for Tmin (minimum air temperature), Tmax (maximum air temperature), Tmean (mean air temperature), and Prec (precipitation), after the gap filling procedure. These montly time series for the 1994-2023 period are available at https://geoportal.mountaingenius.org/portal/. These data, until 2020, were presented in Salerno et al. (2023). In this paper, the last three years have been added to the time series and here we present the results of the last 30 years (1994-2023).

Maximum air temperature (Tmax)

During the warm season (from May to October), Tmax shows a significant negative trend (-0.031 ± 0.015 °C y^{-1}, $p < 0.05$) as highlighted by the progressive $\mu(\tau)$ trend reported in Figure 5a (full line in orange). Increases (although not significant) are observed in November and December; generally, the cold season (from November to April) shows no trend (-0.006 ± 0.013 °C y^{-1}, $p > 0.1$) (full line in blue. Fig. 5a). Considering the annual scale, the trend is negative, but not significant (-0.022 ± 0.011 °C y^{-1}, $p > 0.1$). The decreasing trend seems to have started in 2007 for the warm season, while in the previous years the negative trend was restricted to only May-June-July months, whereas the cold months show trends starting becoming less and less positive from 2011 (Fig.5a) .

Minimum air temperature (Tmin)

November (+0.06 °C y^{-1}, $p < 0.05$) and December (+0.08 °C y^{-1}, $p < 0.01$) present the highest increasing trend, i.e., both months experienced ca. +2.1 °C over thirty years (Fig. 5c). The cold season experienced a positive trend (0.046 ± 0.012 °C y^{-1}, $p < 0.01$) mainly concentrated in the post-monsoon period. As highlighted by the progressive $\mu(\tau)$ trend in Figure 5c (full line in blue), this trend started increasing in 2005. In the warm season, the trend is much lower (+0.024 ± 0.014 °C y^{-1}, $p < 0.1$) and it is negative in May. On the annual scale, the trend is positive (+0.030 ± 0.009 °C y^{-1}, $p < 0.01$).

Mean air temperature (Tmean)

Figure 5b presents intermediate conditions for Tmean. The cold season shows increasing trends, although not significant (0.020 ± 0.009 °C y^{-1}, $p > 0.1$), and only November and December significantly rise. In the warm season, there is no trend (0.003 ± 0.010 °C y^{-1}, $p > 0.1$), while the temperature in May decreases. Also considering the annual scale, there is no trend in the last 30 years (0.005 ± 0.007 °C y^{-1}, $p > 0.1$).

Total precipitation (Prec)

In the last years, for all months of the warm season, an overall and strongly significant decreasing trend of Prec has occurred (Fig. 5d). Considering all periods, a continuous decreasing trend has occurred since 2000, which became significant at the beginning of 2005. The decreasing Prec trend is highest in August. During the warm season, the reduction of precipitation has been 5.9 ± 4.4 mm y-1 (i.e., -41%) (1994-2023).

5 Discussion of the reconstructed time series

Our measurements reveal a local diurnal cooling mainly occurring during the warm season (from May to October), which is in stark contrast to the postulated temperature increases. An interpretation of this phenomenon was provided recently by Salerno et al. (2023). Thus, through the use of this unique dataset and the consistent acquisition of measurements in such a logistically complex area, we managed to provide new insights into the climate dynamics at the highest Himalayan elevations, which would not have been possible relying solely on climatic data from lower elevations.

Conclusion

Glaciers in Himalaya are a major focus of international research, because of their relevance for water and people, their role in climate-land feedbacks, and their iconic (and not entirely understood) patterns of changes. One of the major drawbacks in Himalayan research of the cryosphere is that there are almost no long-term climate measurements at high elevations, where glaciers are located. Here, we presented meteoclimatic data acquired by 7 meteorological stations belonging to the Pyramid Meteorological Network managed by EV-K2-CNR. In this framework, we presented precipitation and temperature time series based on a three-decade effort to ensure a continuous monitoring of the high-elevation climate in Himalaya.

We are convinced that making this data available will open new perspectives on climate change and its effects in Himalaya that will guide research at high elevations in the coming decades

Data availability

All datasets described and presented in this paper can be freely accessed from https://geoportal.mountaingenius.org/portal/. Moreover, the dataset can be downloaded from https://zenodo.org/records/15211352 (Salerno et al., 2024) and distributed under the CCBY4.0 license.

Competing interests

The authors declare that they have no conflict of interest.

Special issue statement

This article is part of the special issue “Hydrometeorological data from mountain and alpine research catchments”. It is not associated with a conference.

Author contribution

F.S., N.G. and N.C. drafted the article, G.T. contributed to improving the manuscript, M.T.M. and F.D. built the Geonetwork platform, N.G. assured the data quality assessment, G.V. and K.B. are responsible for the management of the weather stations.

Acknowledgements

The Pyramid Meteorological Network was supported by the MIUR (Ministero dell'Istruzione e del Merito) through Ev-K2-CNR/SHARE and CNR-DTA/NEXTDATA project within the framework of the Ev-K2-CNR and Nepal Academy of Science and Technology (NAST). NC was supported by the project NODES, which received funding from the MUR–M4C2 1.5 of PNRR funded by the European Union - NextGeneration EU (Grant agreement no. ECS00000036). We are grateful to the Editor and three reviewers who provided valuable feedback and input during the discussion of this manuscript.

References

Abebe, A., Solomatine, D., and Venneker, R.: Application of adaptive fuzzy rule based models for reconstruction of missing precipitation events, Hydrolog. Sci. J., 45, 425–436, https://doi.org/https://doi.org/10.1080/02626660009492339, 2000. https://doi.org/

Abudu, S., Bawazir, A. S., and King, J. P.: Infilling missing daily evapotranspiration data using neural networks, J. Irrig. Drain. E-asce, 136, 317–325, https://doi.org/https://doi.org/10.1061/(ASCE)IR.1943-4774.0000197, 2010.

Amatya, L. K., Cuccillato, E., Haack, B., Shadie, P., Sattar, N., Bajracharya, B., Shrestha, B. Caroli, P., Panzeri, D., Basani, M., Schommer, B., Flury, B. Salerno, F., and Manfredi, E. C.: Improving communication for management of social-ecological systems in high mountain areas: Development of methodologies and tools – The HKKH Partnership Project, Mt. Res. Dev., 30, 69-79, https://doi.org/https://doi.org/10.1659/MRD-JOURNAL-D-09-00084.1, 2010.

Bertolani L., Bollasina, M., and Tartari, G.: Recent biannual variability of meteorological features in the Eastern Highland Himalayas, Geophys. Res. Lett., 27, 2185-2188,

https://doi.org/https://doi.org/10.1029/1999GL011198, 2000.
Bhattacharya, A., Bolch, T., Mukherjee, K., King, O., Menounos, B., Kapitsa, V., ... and Yao, T.:. High Mountain Asian glacier response to climate revealed by multi-temporal satellite observations since the 1960s. Nature Commun., 12(1), 4133., https://doi.org/10.1038/s41467-021-24180-y, 2021.
Bhuju, D. R., Carrer, M., Gaire, N. P., Soraruf, L., Riondato, R., Salerno, F., & Maharjan, S. R.: Dendroecological study of high altitude forest at Sagarmatha National Park, Nepal. Contemporary research in Sagarmatha (Mt. Everest) region, Nepal, 119-130, 2010.
Biemans, H., Siderius, C., Lutz, A. F., Nepal, S., Ahmad, B., Hassan, T., ... and Immerzeel, W. W.: Importance of snow and glacier meltwater for agriculture on the Indo-Gangetic Plain. Nat. Sustain., 2(7), 594-601, https://doi.org/10.1038/s41893-019-0305-3, 2019.
Bocchiola, D. and Diolaiuti, G.: Evidence of climate change within the Adamello Glacier of Italy, Theor. Appl. Climatol., 100, 351–369, https://doi.org/10.1007/s00704-009-0186-x, 2010.
Coulibaly, P. and Evora, N.: Comparison of neural network methods for infilling missing daily weather records, J. Hydrol., 341, 27–41, https://doi.org/10.1016/j.jhydrol.2007.04.020, 2007.
Déqué, M.: Frequency of precipitation and temperature extremes over France in an anthropogenic scenario: model results and statistical correction according to observed values, Global Planet. Change, 57, 16–26, https://doi.org/10.1016/j.gloplacha.2006.11.030, 2007.
Gerstengarbe, F. W. and Werner, P. C.: Estimation of the beginning and end of recurrent events within a climate regime, Clim. Res., 11, 97-107, https://doi.org/10.3354/cr011097, 1999.
Guyennon, N., Romano, E., Portoghese, I., Salerno, F., Calmanti, S., Petrangeli, A. B., Tartari, G., and Copetti, D.: Benefits from using combined dynamical-statistical downscaling approaches – lessons from a case study in the Mediterranean region, Hydrol. Earth Syst. Sc., 17, 705–720, https://doi.org/10.5194/hess-17-705-2013, 2013.
Ichiyanagi, K., Yamanaka, M. D., Muraji, Y., and Vaidya, B. K.: Precipitation in Nepal between 1987 and 1996, Int. J. Climatol., 27, 1753–1762, https://doi.org/10.1002/joc.1492, 2007.
James, A. L. and Oldenburg, C. M.: Linear and Monte Carlo uncertainty analysis for subsurface contaminant transport simulation, Water Resour. Res., 33, 2495–2508, https://doi.org/10.1029/97WR01925, 1997.
Kattel, D. B. and Yao, T.: Recent temperature trends at mountain stations on the southern slope of the central Himalayas, J. Earth Syst. Sci., 122, 215–227, https://doi.org/ 10.1007/s12040-012-0257-8, 2013.
Kattel, D. B., Yao, T., Yang, K., Tian, L., Yang, G. and Joswiak, D.: Temperature lapse rate in complex mountain terrain on the southern slope of the central Himalayas, Theor. Appl. Climatol., 113, 671-682, https://doi.org/10.1007/s00704-012-0816-6, 2013.

Kendall, M.G.: Rank Correlation Methods, Oxford University Press, New York, 1975.

Lin, C., Yang, K., Chen, D., Guyennon, N., Balestrini, R., Yang, X., ... and Salerno, F.: Summer afternoon precipitation associated with wind convergence near the Himalayan glacier fronts. Atmospheric Research, 259, 105658, https://doi.org/10.1016/j.atmosres.2021.105658, 2021.

Locci, F., Melis, M.T., Dessì, F., Stocchi, P., Akinde, M.O., Bønes, V., Bonasoni, P., and Vuillermoz, E.: Implementation of a webGIS service platform for high mountain climate research: the SHARE GeoNetwork project. Geosci. Data J., 1: 140-157. https://doi.org/10.1002/gdj3.14, 2014.

Magnani, A., Ajmone-Marsan, F., D'Amico, M., Balestrini, R., Viviano, G., Salerno, F., and Freppaz, M.: Soil properties and trace elements distribution along an altitudinal gradient on the southern slope of Mt. Everest, Nepal. Catena, 162, 61-71, https://doi.org/10.1016/j.catena.2017.11.015, 2018.

Matthews, T., Perry, B., Khadka, A., Sherpa, T. G., Shrestha, D., Aryal, D., & Alexiev, N. (2022). Weather observations reach the summit of Mount Everest. *Bulletin of the American Meteorological Society*, *103*(12), E2827-E2835.

Melis M. T., Dessì F., Locci F., Bonasoni P. and Vuillermoz E.: Share Geonetwork: a web-service platform for environmental data sharing, Proc. SPIE 8795, First International Conference on Remote Sensing and Geoinformation of the Environment (RSCy2013), 87951V (August 5, 2013); https://doi.org/10.1117/12.2027602. 2013.

Pandey, J., Sigdel, S. R., Lu, X., Salerno, F., Dawadi, B., Liang, E., & Camarero, J. J.: Early growing-season precipitation drives radial growth of alpine juniper shrubs in the central Himalayas. Geografiska annaler: series a, physical geography, 102(3), 317-330, https://doi.org/10.1080/04353676.2020.1761097, 2020.

Pepin, N., Bradley, R.S., Diaz, H.F., Baraer, M., Caceres, E.B., Forsythe, N., … and Yang, D.Q.: Elevation-dependent warming in mountain regions of the world. Nature Climate Change 5:5 5, 424–430. https://doi: 10.1038/ nclimate2563, 2015.

Potter, E. R., Orr, A., Willis, I. C., Bannister, D., & Salerno, F.: Dynamical drivers of the local wind regime in a Himalayan valley. J. Geophys. Res. Atmos. 123(23), 13-186, https://doi.org/10.1029/2018JD029427, 2018.

Salerno, F., Cuccillato, E., Caroli, P., Bajracharya, B., Manfredi, E. C., Viviano, G., Thakuri, S., Flury, B., Basani, M., Giannino, F., and Panzeri, D.: Experience with a hard and soft participatory modeling framework for social ecological system management in Mount Everest (Nepal) and K2 (Pakistan) protected areas, Mt. Res. Dev., 30, 80-93, https://doi.org/10.1659/MRD-JOURNAL-D-10-00014.1, 2010.

Salerno, F., Guyennon, N., Thakuri, S., Viviano, G., Romano, E., Vuillermoz, E., ... and Tartari, G.: Weak precipitation, warm winters and springs impact glaciers of south slopes of Mt. Everest (central Himalaya) in the last 2 decades (1994–2013). The Cryosphere, 9(3), 1229-1247, https://doi.org/10.5194/tc-9-1229-2015, 2015.

Salerno, F., Guyennon, N., Yang, K., Shaw, T. E., Lin, C., Colombo, N., ... and Pellicciotti, F.: Local cooling and drying induced by Himalayan glaciers under global warming. Nat. Geosci., 16(12), 1120-1127, https://doi.org/10.1038/s41561-023-01331-y, 2023.

Salerno, F., Thakuri, S., Tartari, G., Nuimura, T., Sunako, S., Sakai, A., and Fujita, K.: Debris-covered glacier anomaly? Morphological factors controlling changes in the mass balance, surface area, terminus position, and snow line altitude of Himalayan glaciers. Earth Planet. Sci. Lett., 471, 19-31, https://doi.org/10.1016/j.epsl.2017.04.039, 2017.

Salerno, F., Guyennon, N., Colombo, N., Melis, M. T., Dessì, F. G., Verza, G., Bista, K., Sheharyar, A., and Tartari, G. (2024). Pyramid Meteorological Network - EVK2CNR (Version 1) [Data set]. Zenodo https://zenodo.org/records/15211352.

Schneider, T.: Analysis of incomplete climate data: Estimation of mean values and covariance matrices and imputation of missing values, J. Clim., 14, 853–871, https://doi.org/10.1175/1520-0442(2001)014<0853:AOICDE>2.0.CO;2, 2001.

Sen, P. K.: Estimates of the regression coefficient based on Kendall's Tau, J. Am. Assoc., 63, 1379-1389, https://doi.org/10.2307/2285891, 1968.

Shea, J. M., Immerzeel, W. W., Wagnon, P., Vincent, C., & Bajracharya, S.: Modelling glacier change in the Everest region, Nepal Himalaya. The Cryosphere, 9(3), 1105-1128., https://doi.org/10.5194/tc-9-1105-2015, 2015.

Shrestha, A. B., Wake, C. P., Mayewski, P. A., and Dibb, J. E.: Maximum temperature trends in the Himalaya and its vicinity: An analysis based on temperature records from Nepal for the period 1971-94, J. Clim., 12, 2775-5561, https://doi.org/10.1175/1520-0442(1999)012<2775:MTTITH>2.0.CO;2, 1999.

Sigdel, S. R., Pandey, J., Liang, E., Muhammad, S., Babst, F., Leavitt, S. W., ... and Peñuelas, J.: No benefits from warming even for subnival vegetation in the central Himalayas. Sci Bull, 66(18), 1825-1829, 2021.

Tartari, G., Salerno, F., Buraschi, E., Bruccoleri, G., and Smiraglia, C.: Lake surface area variations in the North-Eastern sector of Sagarmatha National Park (Nepal) at the end of the 20th Century by comparison of historical maps, J. Limnol., 67, 139-154, https://doi.org/10.4081/jlimnol.2008.139, 2008.

Thakuri, S., Salerno, F., Bolch, T., Guyennon, N., & Tartari, G.: Factors controlling the accelerated expansion of Imja Lake, Mount Everest region, Nepal. Ann. Glaciol., 57(71), 245-257., 2016.

Thakuri, S., Salerno, F., Smiraglia, C., Bolch, T., D'Agata, C., Viviano, G., and Tartari, G.: Tracing glacier changes since the 1960s on the south slope of Mt. Everest (central southern Himalaya) using optical satellite imagery, The Cryosphere, 8, 1297-1315, https://doi.org/10.5194/tc-8-1297-2014, 2014.

Themeßl, M. J., Gobiet, A., and Heinrich, G.: Empirical-statistical downscaling and error correction of regional climate models and its impact on the climate change signal, Climatic Change, 112, 449-468, https://doi.org/10.1007/s10584-011-011-0224-4, 2012.

The GlaMBIE Team: Community estimate of global glacier mass changes from 2000 to 2023. Nature 639, 382–388. https://doi.org/10.1038/s41586-024-08545-z, 2025.

Ueno, K., K. Toyotsu, L. Bertolani, and G. Tartari: Stepwise onset of monsoon weather observed in the Nepal Himalaya. Mon. Wea. Rev., 136, 2507-2522,

https://doi.org/10.1175/2007MWR2298.1, 2008
Yang, K., Guyennon, N., Ouyang, L., Tian, L., Tartari, G., and Salerno, F.: Impact of summer monsoon on the elevation-dependence of meteorological variables in the south of central Himalaya. International J.Clim., 38(4), 1748-1759, https://doi.org/10.1002/joc.5293, 2018.
Yao, T., Bolch, T., Chen, D., Gao, J., Immerzeel, W., Piao, S., ... and Zhao, P.: The imbalance of the Asian water tower. Nat. Rev. Earth Environ., 3(10), 618-632, https://doi.org/10.1038/s43017-022-00299-4, 2022.
Wagnon, P., Brun, F., Khadka, A., Berthier, E., Shrestha, D., Vincent, C., ... and Jomelli, V.: Reanalysing the 2007–19 glaciological mass-balance series of Mera Glacier, Nepal, Central Himalaya, using geodetic mass balance. J.Glaciol., 67(261), 117-125, https://doi.org/10.1017/jog.2020.88, 2021.

Table 1. List of stations belonging to the Pyramid Meteorological Network.

Station ID	Location	Latitude ° N	Longitude °E	Elevation m a.s.l.	Mean feature of the landscape	Sampling rate
AWSSC	South Col	27.98	86.92	7 986	Mountain peak (off glacier)	1 hour
CNG_SNP	Changri Nup	27.98	86.77	5 700	Glacier (on glacier)	1 hour
AWS4	Kala Patthar	27.99	86.83	5 600	Mean glaciers surface (off glacier)	1 hour
AWS0, AWS1	Pyramid	27.96	86.81	5 035	Mean glacier fronts (off glacier)	2 hour/1 hour
AWS2	Pheriche	27.90	86.82	4 260	Treeline (off glacier)	1 hour
AWS5	Namche	27.80	86.71	3 570	Forests (off glacier)	1 hour
AWS3	Lukla	27.70	86.72	2 660	Forests (off glacier)	1 hour

Table 2. Percentage of daily missing data for each variable. AT: 2m Atmospheric Temperature (°C); RR: Rainfall Rate (mm); RH: Relative Humidity (%); AP: Atmospheric Pressure (hPa); WS: Wind Speed (m/s); WD: Wind Direction (°). The Z naming convention relates to elevation of each station.

Station ID	AP	AT	RH	RR	WD	WS	UVA
Z7986	54	61.8	78	-	67.9	64.9	46,6
Z5700	-	6	6	-	25.6	25.1	-

Z5600	16.5	18.1	18.9	44.6	26.9	28.2	-
Z5035 (AWS0)	12.6	18.1	18.5	23.3	53.4	12.6	-
Z5035 (AWS1)	7.2	6.8	22.3	9.4	10.5	9.1	-
Z4260	13	15.3	14.4	14.8	20.2	23.3	-
Z3570	39	41.9	53.1	42.9	43.7	42.5	-
Z2660	49.1	51	63	52.1	54	49.4	-

Table 3. List of sensors with measurement height, manufacturer, and accuracy. The Z naming convention relates to elevation of each station.

Parameter	Sensor	Manufacturer	Accuracy
	AWSSC(Z7986)		
Air temperature	Thermoresistance (2m)	Lsi-Lastem /Vaisala	0.1°C/0.3°C
Precipitation	Tipping Bucket (1.5m)	Lsi-Lastem	2%
Relative humidity	Capacitive Plate (2m)	Lsi-Lastem /Vaisala	1.5%/2.5%
Atmospheric pressure	Slice of Silica (2m)	Lsi-Lastem /Vaisala	1hPa/0.5 hPa
	CNG_SNP(Z5700)		
Air temperature	Thermoresistance (2m)	Lsi-Lastem /Vaisala	0.1°C/0.3°C
Precipitation	Tipping Bucket (1.5m)	Lsi-Lastem	2%
Relative humidity	Capacitive Plate (2m)	Lsi-Lastem /Vaisala	1.5%/2.5%
Atmospheric pressure	Slice of Silica (2m)	Lsi-Lastem /Vaisala	1hPa/0.5 hPa
	AWS4(Z5600035)		
Air temperature	Thermoresistance (2m)	Lsi-Lastem	0.1°C
Precipitation	Tipping Bucket (1.5m)	Lsi-Lastem	1%
Relative humidity	Capacitive Plate (2m)	Lsi-Lastem	1.5%
Atmospheric pressure	Slice of Silica (2m)	Lsi-Lastem	1hPa
	AWS0 (Z5035)		
Air temperature	Precision Linear Thermistor (2m)	MTX	0.1°C
Precipitation	Tipping Bucket (1.5m)	MTX	0.2 mm
Relative humidity	Solid state hygrometer (2m)	MTX	3%
Atmospheric pressure	Aneroid capsule (2m)	MTX	0.5hPa
	AWS1(Z5035)		
Air temperature	Thermoresistance (2m)	Lsi-Lastem	0.1°C
Precipitation	Tipping Bucket (1.5m)	Lsi-Lastem	2%
Relative humidity	Capacitive Plate (2m)	Lsi-Lastem	2.5%
Atmospheric pressure	Slice of Silica (2m)	Lsi-Lastem	1hPa
	AWS2(Z4260)		
Air temperature	Thermoresistance (2m)	Lsi-Lastem /Vaisala	0.1°C/0.3°C
Precipitation	Tipping Bucket (1.5m)	Lsi-Lastem	2%
Relative humidity	Capacitive Plate (2m)	Lsi-Lastem /Vaisala	1.5%/2.5%
Atmospheric pressure	Slice of Silica (2m)	Lsi-Lastem /Vaisala	1hPa/0.5 hPa
	AWS5(Z3570)		
Air temperature	Thermoresistance (2m)	Lsi-Lastem	0.1°C
Precipitation	Tipping Bucket (1.5m)	Lsi-Lastem	2%
Relative humidity	Capacitive Plate (2m)	Lsi-Lastem	2.50%
Atmospheric pressure	Slice of Silica (2m)	Lsi-Lastem	1hPa
	AWS3(Z2660)		
Air temperature	Thermoresistance (2m)	Lsi-Lastem	0.1°C/0.3°C

Precipitation	Tipping Bucket (1.5m)	/Vaisala Lsi-Lastem	2%
Relative humidity	Capacitive Plate (2m)	Lsi-Lastem /Vaisala Lsi-Lastem	1.5%/2.5%
Atmospheric pressure	Slice of Silica (2m)	/Vaisala	1hPa/0.5 hPa

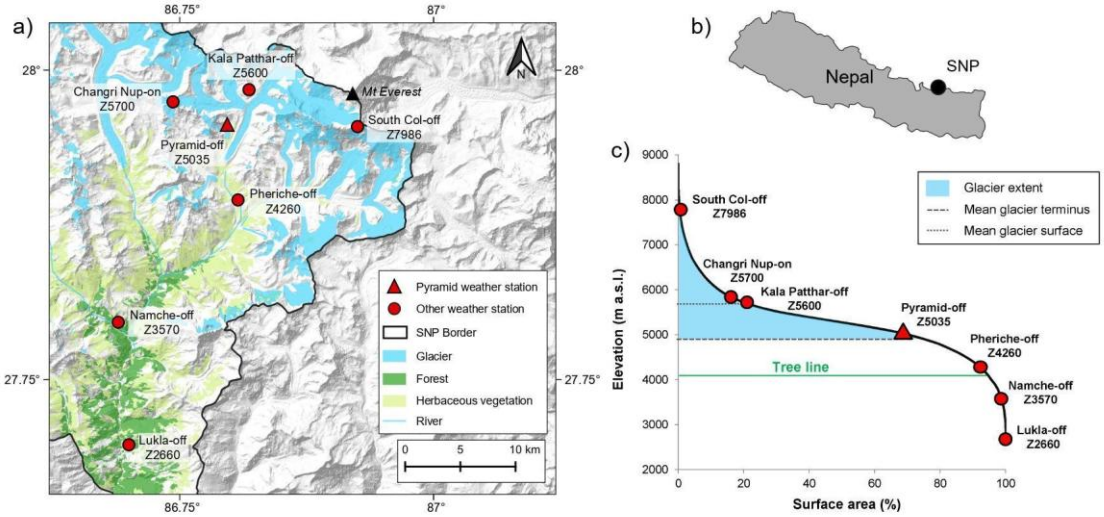

Figure 1. a and b) Location of meteorological monitoring network in the Sagarmatha National Park (SNP), Nepal. c) Hypsometric curve of the SNP and altitudinal glacier distribution. Along this curve, the locations of meteorological stations belonging to the Pyramid Observatory Laboratory are presented.

Figure 2. Photographs of the Pyramid Meteorological Network.

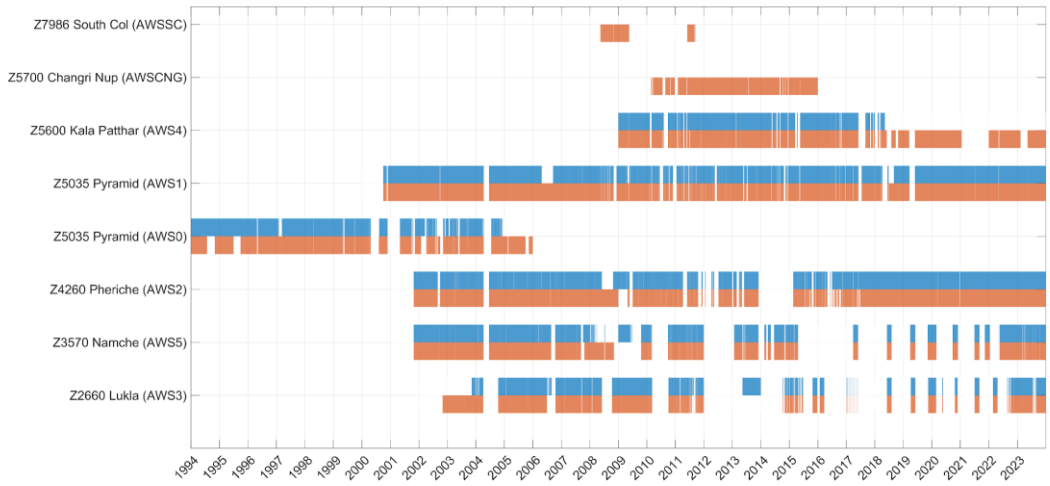

Figure 3. Available data time series (precipitation: blue; temperature: orange) for the Pyramid Meteorological Network since 1994.

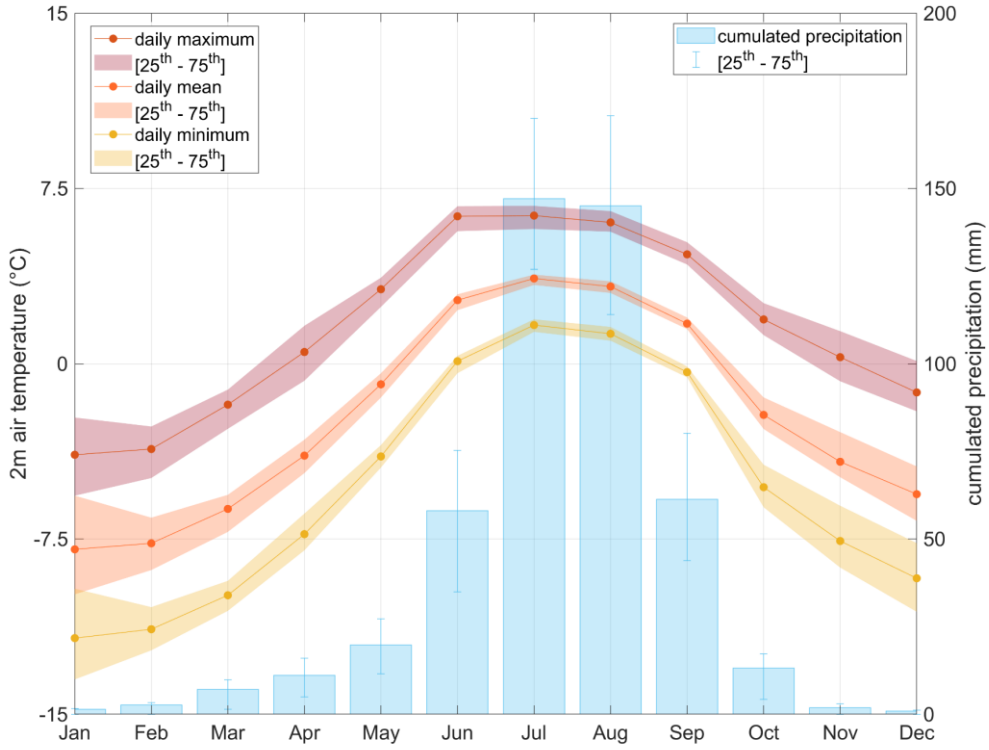

Figure 4. Mean monthly cumulative precipitation and minimum, maximum, and mean temperature at Pyramid station (5035 m a.s.l.; reference period 1994–2023).

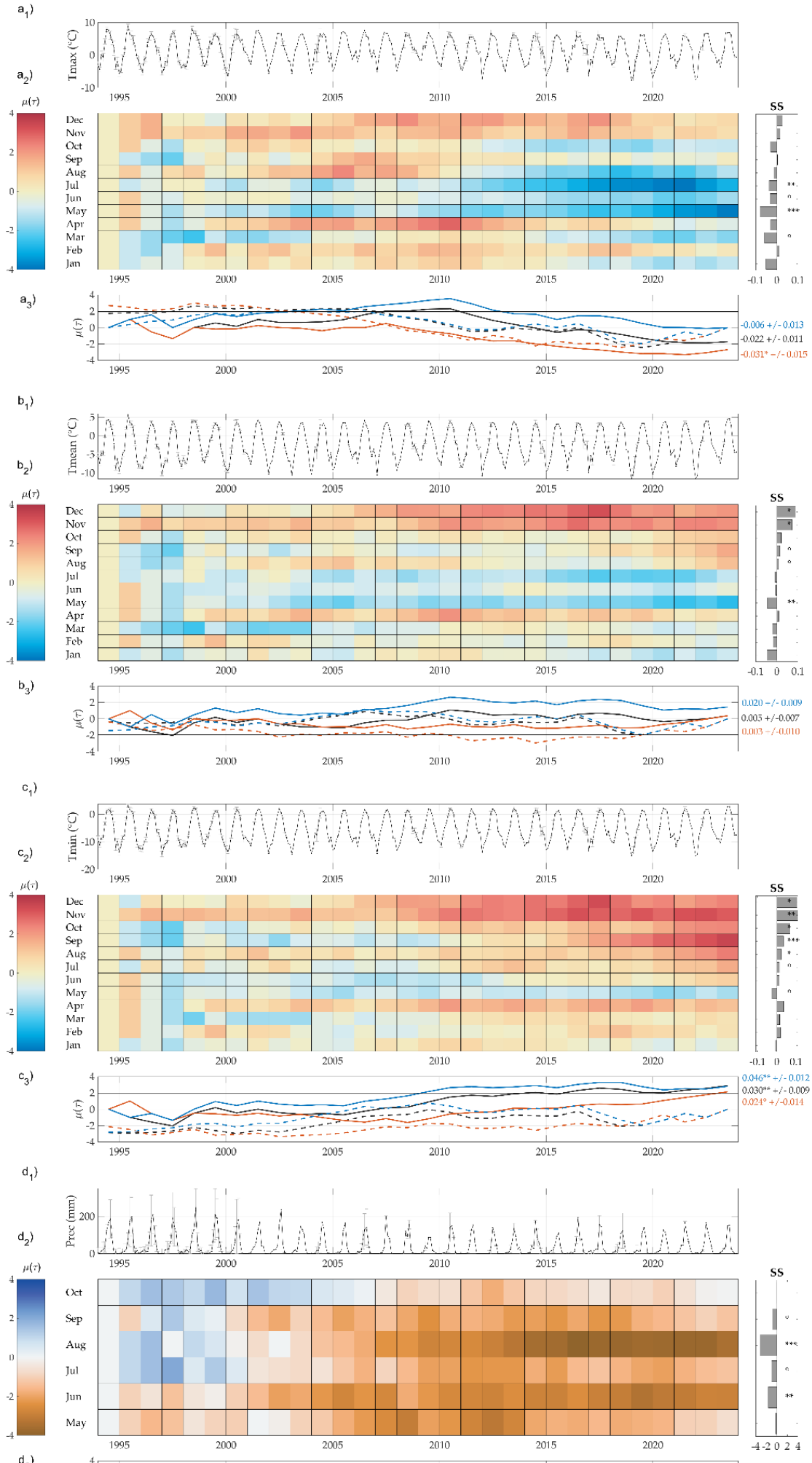
a1)
a2)
a3)
b1)
b2)
b3)
c1)
c2)
c3)
d1)
d2)
d3)
Tmax (°C)
Tmean (°C)
Tmin (°C)
Prec (mm)
μ(τ)
SS
Dec
Nov
Oct
Sep
Aug
Jul
Jun
May
Apr
Mar
Feb
Jan
1995
2000
2005
2010
2015
2020
-0.006 +/- 0.013
-0.022 +/- 0.011
-0.031* +/- 0.015
0.020 +/- 0.009
0.005 +/-0.007
0.003 +/-0.010
0.046** +/- 0.012
0.030** +/- 0.009
0.021° +/-0.014

*Figure 5. Air temperature and precipitation trend analysis at Pyramid station (5035 m a.s.l.): a) maximum, b) mean, c) minimum temperature, and d) total precipitation. The top graph of each meteorological variable (from a to d) shows the monthly time series. The grids display the results of the MK test applied at the monthly scale and calculated from the beginning of the series to the given year. The colour bar represents the normalized Kendall's tau coefficient μ(τ). The colour tones below −1.96 and above 1.96 are significant (α = 5%). On the right, the monthly Sen's Slope (SS) and the significance levels for 1994–2023 ($^{o}p < 0.1$, *p < 0.05, ** p < 0.01, *** p < 0.001). The bottom graph plots show the progressive μ(τ) (solid lines) and retrograde (dotted line) of the seqMK test (calculated from the beginning or from the end, respectively, of the series to the given year) for the cold season (November-April) (blue), the warm season (May-October) (orange), and for the entire year (black). For each year, below-zero lines indicate negative trends (calculated from 1994).*